ADVANCED MATERIALS INTERFACES
www.advmatinterfaces.de

Correlating Surface Plasmon Resonance Microscopy of Living and Fixated Cells with Electron Microscopy Allows for Investigation of Potential Preparation Artifacts

Eva Kreysing, Silke Seyock, Hossein Hassani, Elke Brauweiler-Reuters, Elmar Neumann, and Andreas Offenhäusser**

The investigation of the cell–substrate interface is of great importance for a broad spectrum of areas such as biomedical engineering, brain-chip interfacing, and fundamental research. Due to its unique resolution and the prevalence of instruments, electron microscopy (EM) is used as one of the standard techniques for the analysis of the cell–substrate interface. However, possible artifacts that might be introduced by the required sample preparation have been the subject of speculation for decades. Due to recent advances in surface plasmon resonance microscopy (SPRM), the technique now offers a label-free alternative for the interface characterization with nanometer resolution in axial direction. In contrast to EM, SPRM studies do not require fixation and can therefore be performed on living cells. Here, a workflow that allows for the quantification of the impact of chemical fixation on the cell–substrate interface is presented. These measurements confirm that chemical fixation preserves the average cell–substrate distances in the majority of studied cells. Furthermore, it is possible to correlate the SPRM measurements with EM images of the cell–substrate interface of the exact same cells, thus identifying regions of good agreement between the two methods and revealing artifacts introduced during further sample preparation.

1. Introduction

Understanding the interaction of cells with artificial materials is essential for fundamental research as well as biomedical applications such as cell and tissue engineering, the design of implants and prosthesis but also in the development of brain–computer interfaces.[1–5] Surface modifications such as nanostructures and coatings can act as chemical, mechanical, and topological cues that influence cell–substrate adhesion, cell migration and even stem cell fate.[2,6,7] In the development of implants such as retina implants, a strong cell–substrate adhesion is crucial for a good cell-electrode communication while mediating a good integrity.[8–10] Understanding said interactions requires sophisticated imaging techniques with a resolution in the nanometer range. This makes electron microscopy (EM) an indispensable tool in the field. EM includes multiple different techniques such as transmission electron microscopy (TEM)[11–14] and scanning (transmission) electron microscopy (S(T)EM).[15–28]

While S(T)EM can reach nanometer resolution, it requires extensive sample preparation prior to the FIB sectioning. As a first step, the cells are usually fixated using a crosslinker such as glutaraldehyde which crosslinks proteins and preserves the cell structure. Volumetric studies showed that depending on the protocol, glutaraldehyde fixation might either preserve or change the cell volume in single cells[29] whereas shrinkage was reported when fixating corneal endothelial tissue.[30] However, the impact on the cell–substrate distance in the nanometer range has so far not been studied but it could help interpret EM images of the cell–substrate interface correctly.

Two frequently used preparation techniques are critical point drying (CPD) and resin embedding.[7,21,31,32] In CPD, the chemical fixation is followed by a dehydration of the cell. Intracellular water is exchanged with ethanol and subsequently replaced with liquid CO_2, which is afterward transferred into a supercritical fluid and blown off. This can be followed by heavy metal stainings which allow for resolution of the cellular ultrastructure in EM.

In resin embedding protocols, chemical fixation is often followed by heavy metal stainings, e.g., with OsO_4 and uranyl acetate. Subsequently, the intracellular water is replaced by a

Dr. E. Kreysing, H. Hassani, E. Brauweiler-Reuters, Prof. A. Offenhäusser
Forschungszentrum Jülich GmbH
Institute of Complex Systems
Bioelectronics (ICS-8) 52425 Jülich, Germany
E-mail: emk42@cam.ac.uk; a.offenhaeusser@fz-juelich.de
Dr. E. Kreysing
Department of Physiology
Development and Neuroscience (PDN)
University of Cambridge
Downing Street, CB2 3DY Cambridge, UK
Dr. S. Seyock
Klinik und Poliklinik für Anästhesiologie und Intensivmedizin
AG IRIS
Universitätsmedizin Rostock Schillingallee 69, 18057 Rostock, Germany
Dr. E. Neumann
Forschungszentrum Jülich GmbH
Helmholz Nanofacility (HNF), 52425 Jülich, Germany
The ORCID identification number(s) for the author(s) of this article can be found under https://doi.org/10.1002/admi.201901991.

DOI: 10.1002/admi.201901991

solvent, e.g., ethanol and afterward by resin which mechanically stabilizes the cell structure during FIB sectioning. In order to identify individual cells in EM, excess resin needs to be removed, preserving only the resin within the cell and a thin layer on top which is afterward polymerized by heat (thin layer plastification (TLP)). Whilst CPD can be carried out relatively quickly, resin embedding is usually more time-consuming and often requires the handling of toxic and radioactive substances. The two methods also differ regarding the artifacts that they introduce. On the one hand, CPD can produce drying artifacts like volume shrinkage of the cells[33–36] and a porous structure at the interface.[21,23,37] On the other hand, the exchange of water against a solvent in resin embedding protocols may produce dehydration artifacts which might be less obvious in EM images because the resin only stabilizes the structure that has been obtained after the dehydration step.[21,38]

There are several optical techniques that in contrast to EM offer the opportunity to investigate the interface of the living cell. Examples are fluorescence interference contrast microscopy (FLIC)[39,40] and metal induced energy transfer (MIET).[41] These techniques can be used to study the interface between the fluorescent labeled cell membrane and the specific substrate. The calculation of the cell–substrate distance in FLIC and MIET is based on the modulation of the fluorescence intensity and the fluorescence lifetime of the dye molecules in the vicinity of specific substrates, respectively.

While the axial resolution can reach nanometer accuracy, the lateral resolution of FLIC and MIET has been reported to reach an accuracy of up to 900 and 200 nm, respectively. These techniques allow for insights into the living cell, but they might affect the cellular behavior as fluorescent dyes can be cytotoxic. [42,43]

Surface plasmon resonance microscopy (SPRM) represents a label-free technique allowing for the study of the cell–substrate interface. Widefield SPRM is based on the illumination of the interface at a single but adjustable incidence angle, which enables imaging of the interface in real time.[44–56] This has been demonstrated to resolve cell adhesion complexes as well as other subcellular structures.[50,52,57]

In scanning SPRM, the incident light is focused at the cell–substrate interface, resulting in a spotwise sample illumination with a wide range of angles. Afterward, the intensity of the reflected light over the angle spectrum is analyzed to quantitatively determine the cell–substrate distance as well as the intracellular refractive index (RI). Since scanning SPRM permits a label-free measurement of the cell–substrate distance in living cells with similar lateral resolution to MIET while avoiding phototoxicity, it has been proven to be a valuable alternative to the above optical techniques.[44,49,58] Due to recent improvements to the analysis routine, SPRM can now also reach an accuracy of up to 1.5 nm in axial direction,[56] which is comparable to FLIC, MIET and EM.

Correlative studies of EM with techniques which study the cell–substrate interface in vitro have the potential to reveal artifacts caused by fixation and further preparation and thus help to correctly interpret EM images of the interface. By performing a fixation protocol on a set of cells and measuring each individual cell with SPRM both prior to and after fixation as well as with FIB-S(T)EM, we were able to measure the impact of the chemical fixation on the cell–substrate interface of the investigated cells and to identify artifact affected regions. Correlating these techniques, we can characterize the unperturbed living cell using SPRM, which may even give insights into cellular dynamics,[49,52–54,56,59] while EM images of the FIB-cross-sections allow us to resolve the cell membrane at focal adhesion points of the fixed cell with nanometer resolution in *x*- and *z*-direction. This will help us understand whether the cells, as we see them in EM, differ fundamentally from their state in vitro and whether potential artifacts are caused by fixation or other preparation steps.

2. Results

For this study, we used an objective-based SPRM setup which provides a live-imaging as well as a scanning mode for observing cells cultured on gold-coated glass samples. The live-imaging mode (see **Figure 1**a) is a widefield imaging technique which allows us to observe the cell–substrate contact area qualitatively. Here, areas with a close cell–substrate distance appear relatively bright whereas areas with higher cell–substrate distances and the surrounding of the cell appear darker (see Figures 1b and **2**b,e). The scanning mode (see Figure 1c) is based on a point-wise illumination of the substrate and allows us to quantify the cell–substrate distance as well as the intracellular refractive index (RI) at each point. As described in greater detail in the Experimental Section, we capture one image of the back focal plane (BFP) at each scanning point, extract a reflectance profile (see Figure 1f) from this image and fit a layer model describing the sample structure (Figure 1d). As a result, we can generate a 3D representations of the basal cell membrane as well as RI profiles of the cytosol.[56]

The cells used were primary cortical rat neurons cultured on poly-L-lysine (PLL) coated SPRM substrates and investigated on day in vitro (DIV) 7. We used the SPRM live-imaging mode to localize cells with a good contrast compared to their surrounding and identified their position on the chip using the photo resist markers (see the Experimental Section) before scanning the respective living cells. Afterward, we fixed the cells using glutaraldehyde, washed the samples carefully with phosphate-buffered saline (PBS) and remounted the samples on the setup. Subsequently, the previously scanned cells were localized using the live-imaging mode and scanned with identical settings. Afterward, we stained the samples with osmium tetroxide (OsO4), which binds to the phospholipids in the membrane. Tannic acid is then used to improve the fixation and mediate binding of uranyl acetate which binds to proteins and lipids in the final staining. These steps stabilize the cell membrane and the high atomic weight of the heavy metals leads to a good contrast between the cell membrane and the surrounding resin in EM.[60] This was followed by resin infiltration, removal of the extracellular resin and a polymerization (see the Experimental Section).

Using a FIB-SEM system, we localized the same cells previously characterized with SPRM using photo resist markers and deposited additional platinum layers on the region of interest (see the Experimental Section). The FIB sectioning was started from one side and stopped when the center of the cell

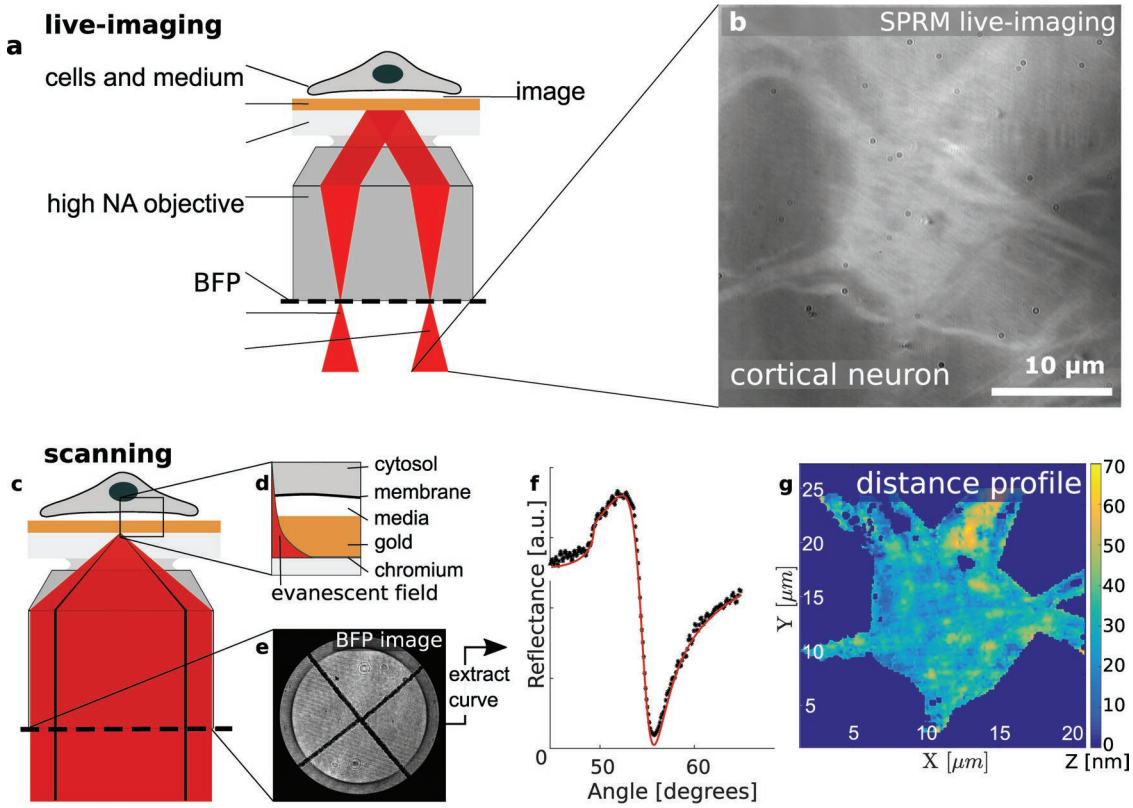

Figure 1. Qualitative and quantitative interface characterization. The SPRM live-imaging and scanning mode allow for a qualitative and a quantitative characterization of the cell–substrate interface, respectively. a) In the live-imaging mode, light is focused on the back focal plane (BFP) of the TIRF objective resulting in an illumination of the cell–substrate interface with parallel light. b) If illuminated under the resonance angle of the bare cell–substrate interface, areas of close cell–substrate distances appear relatively bright while areas with poor adhesion appear relatively dark. c) In the scanning mode, the entire BFP is illuminated with radially polarized light resulting in an illumination of the sample with a broad range of angles. d) Illuminating the sample under angles larger than the critical angle creates an evanescent field penetrating the cytosol. e) Recording the BFP at each scanning point allows for the extraction of the f) reflectance curve. f) Modeling the sample as a multilayer system, we can simulate the reflectance curve. Fitting the model to the data, we can extract the cell–substrate distance. g) Combining the data from the entire set of scanning points, we can reconstruct the 3D structure of the basal cell membrane.

was reached. Afterward, we imaged the cross-section with the integrated SEM system and continued FIB sectioning from the opposite side in order to prepare a thin lamella from the center of the cell. Finally, we soldered said lamella to a lift-out-grid which was then attached to a STEM holder. This sample was mounted in an STEM (STEM-in-SEM system) which allowed us to image the cell–substrate interface with a higher resolution compared to the SEM images.

To determine the changes in cell–substrate distance due to chemical fixation, each SPRM scan was analyzed as described in the Experimental Section. The resulting distance profiles of the living and fixed cells were subtracted. For this task, additional software was written to allow us to align the areas scanned before and after fixation correcting for displacement and rotation of the sample caused by the second sample mounting (for align and compare software, see the Experimental Section). The changes in the distance profiles as well as the RI profile can be displayed in multiple ways:

The area plots shown in Figures 2f and 6f provide information regarding the fixation process in the individual cells. Areas with small variations in the cell–substrate distance indicate that the fixation process has preserved the original structure of the cell–substrate interface (see central areas of the cell in Figure 2f). Areas with large distance variations can indicate that the cell has partially detached from the substrate or collapsed locally during the process. Figure 6f shows strong changes in the cell–substrate distance of up to 60 nm, indicating that the fixation process did not conserve the original structure in the respective areas.

The line plots give quantitative information about the cell–substrate distance along a cross-section between any two points. They enable us to compare the morphology of the cell in cross-section before and after fixation at a glance (**Figure 3**b,d,f). This facilitates the identification of fixation-related artifacts along the selected cross-section. These diagrams, which are chosen in the same direction as the cross-section in FIB sectioning, provide good comparability with EM images of the cell–substrate interface (**Figure 4**b,e). This in turn makes it possible to differentiate between fixation-related artifacts and artifacts resulting from other preparation steps.

Figure 4 demonstrates the correlation of SPRM and EM for two cells. Figure 4a,d shows the results of the SPRM cell–substrate distance measurements in vitro. The dashed lines in Figure 4a,d indicate the cross-sections that are used to evaluate

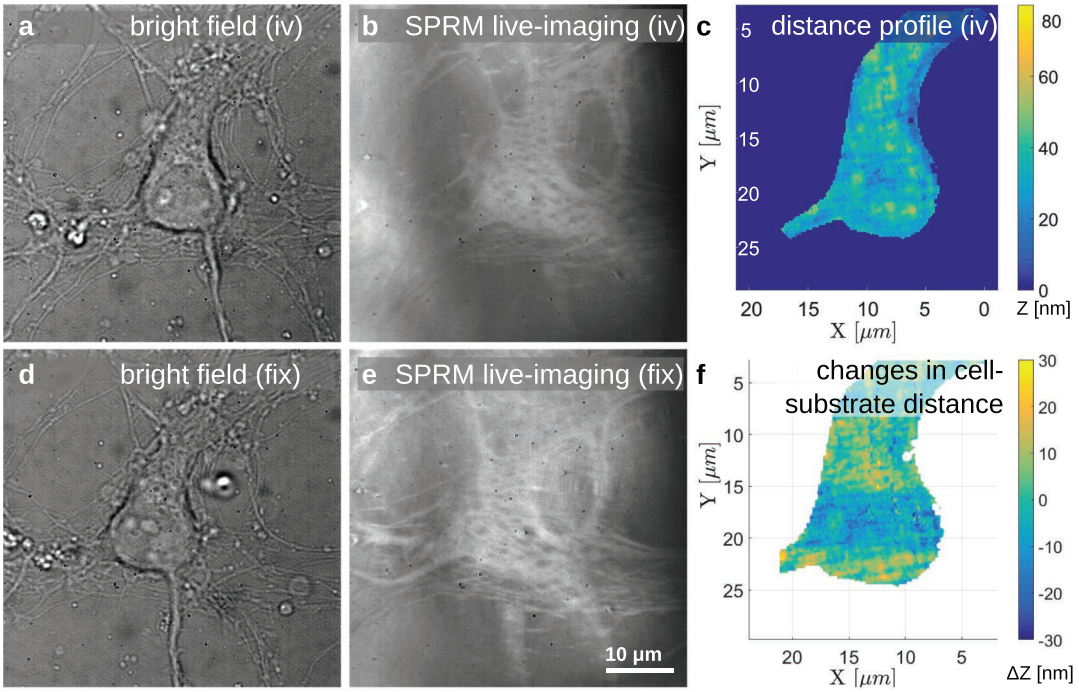

Figure 2. Fixation-induced changes at the interface observed with SPRM. a,d) Bright field images of the neuron give information regarding the shape of the soma and the dendrites in vitro (iv) and fixed (fix), respectively. b,d) The differences in contrast between the background and the adherent areas in the live-imaging of the living and the fixed cell indicate a change at the cell–substrate interface. c) The scanning results reveal the cell–substrate distances (results shown here correspond to the living cell). f) Subtracting the distance profiles of the living and the fixed system reveals the changes in the cell–substrate distances which are induced by the chemical fixation.

the distance profiles shown in Figure 4b,e, respectively. Figure 4c,f shows the SEM images along the same cross-sections as in Figure 4a,d (the contrasts in the SEM images have been inverted). The SEM cross-sections reveal several bright structures at the cell–substrate interface. Since the gray values within these structures are very similar to the gray values of the resin surrounding the cell, it can be concluded that they correspond to resin-filled cavities. As we will discuss later, the cell shown in Figure 4d–f underwent the smallest changes in the cell–substrate distance during the chemical fixation (see **Figure 5**, cell 8). As this result suggests that the morphology of this fixed cell might be close to its physiological state, we chose to image this particular cell using STEM. For this purpose, we prepared a lamella from the center of the cell corresponding to the cross-section shown in Figure 4d. As we can see in Figure 4g–j, the STEM images allow resolution of the cell membrane. Here, the resin appears bright and the cell membrane and the substrate relatively dark.

As we can see in the images recorded after the first sample mounting (Figure 4g,h), the resin was well attached to the substrate. However, after several mountings in the STEM, the fragile lamella disintegrated. Luckily, the resin detached cleanly from the gold surface of the substrate so that we can still investigate the cell–substrate interface. This is why, the surrounding of the resin appears very bright in Figure 4i,j.

Figure 4g shows an area with large adhering areas and small cell–substrate distances. As the separation between the intracellular and the extracellular space seems distinct, we conclude that the membrane is intact. Figure 4h instead shows a large oval structure close to the interface which resembles a vacuole. Here, we cannot tell with certainty whether this structure is closed or the membrane is torn. Therefore, the vacuole could already have been present in the living cell and have been preserved by fixation or introduced by further preparation steps.

Figure 4i,j shows close-ups of two other cavities. While Figure 4i shows a distinct separation of the extracellular and intracellular space by the cell membrane, the edge of the cytosol in Figure 4j appears fuzzy suggesting that the membrane ruptured during the fixation or following preparation steps.

To quantitatively analyze the effect of chemical fixation of multiple cells, we determine the changes in SPRM measurements as described in the Experimental Section. The changes for all scanning points are then pooled for the individual cells and their probability density function estimated (see Figure 5). With the exception of cell 2, the median of the change in cell–substrate distance scatters around 0 nm within an interval of 10 nm without preferential directionality. This shows that the average distance between cell and substrate is maintained for the vast majority of measured cells. As for the changes in cytosolic RI, there is a clear trend toward higher values after fixation, which will be discussed below.

3. Discussion

In order to understand how glutaraldehyde mediated fixation can alter the cell–substrate interface, we will first discuss cell–substrate adhesion under physiological conditions. Then

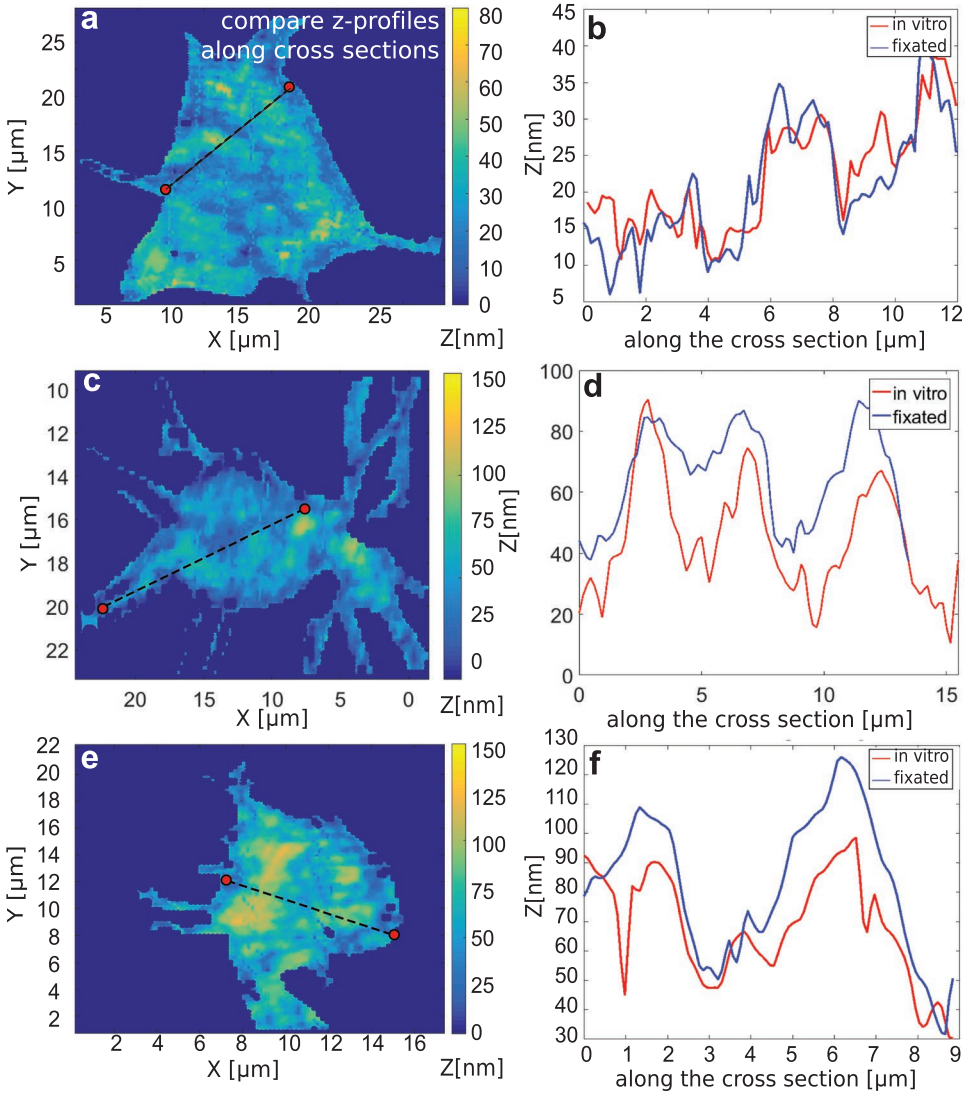

Figure 3. Distance profile along the cross-section measured with SPRM. a,c,e) Definition of the cross-section via graphical input using the software align and compare. b,d,e) The cell–substrate distance is plotted along the chosen cross-section in the states before and after the chemical fixation.

we will address the chemical processes during the fixation processes and how they might introduce changes at the cell–substrate interface.

The cells were seeded on a PLL-coated substrate. As PLL is positively charged under physiological conditions, negatively charged acidic side chains such as aspartic acid or glutamic acid in the membrane proteins can bind electrostatically.[61] The charged proteins in the membrane and cytosol are hydrated due to the polarity of the water molecules in the cytosol and within the culture media. Glutaraldehyde, which is often used in fixation protocols, links amino groups of close by polypeptides.[61] This causes crosslinking of membrane proteins to the PLL coating, however intracellular proteins inside the organelles or the cytoskeleton can also be crosslinked. During the crosslinking, the glutaraldehyde binds covalently to the amino acids of two closely spaced polypeptides. Consequently, amino groups lose their charges, forming a neutral complex with their two binding partners.

In our understanding, the change in charge distribution within the cell proteins might affect the tertiary structure of the proteins. The absence of the charges responsible for the hydration might result in a locally reduced water concentration. The covalent bonds caused by crosslinking are much stronger than the electrostatic interaction responsible for the cell-coating adhesion in the living cell. Assuming that the system evolves in favor of energetically lower states during the incubation time of the crosslinker, we would expect changes in the cell-adhesion complexes when compared to the living cell. The change in the tertiary structure and the hydration of the proteins can also explain local changes in the cell–substrate distance. The observed increase of the cytosolic RI gives evidence for the validity of this explanation: As the RI of water (1.33)[62] is low compared to the RI of proteins (>1.50),[63] a local reduction of water concentration would result in a higher cytosolic RI after the fixation. This explains the fixation-related contrast enhancement that we observed in the live images. Since

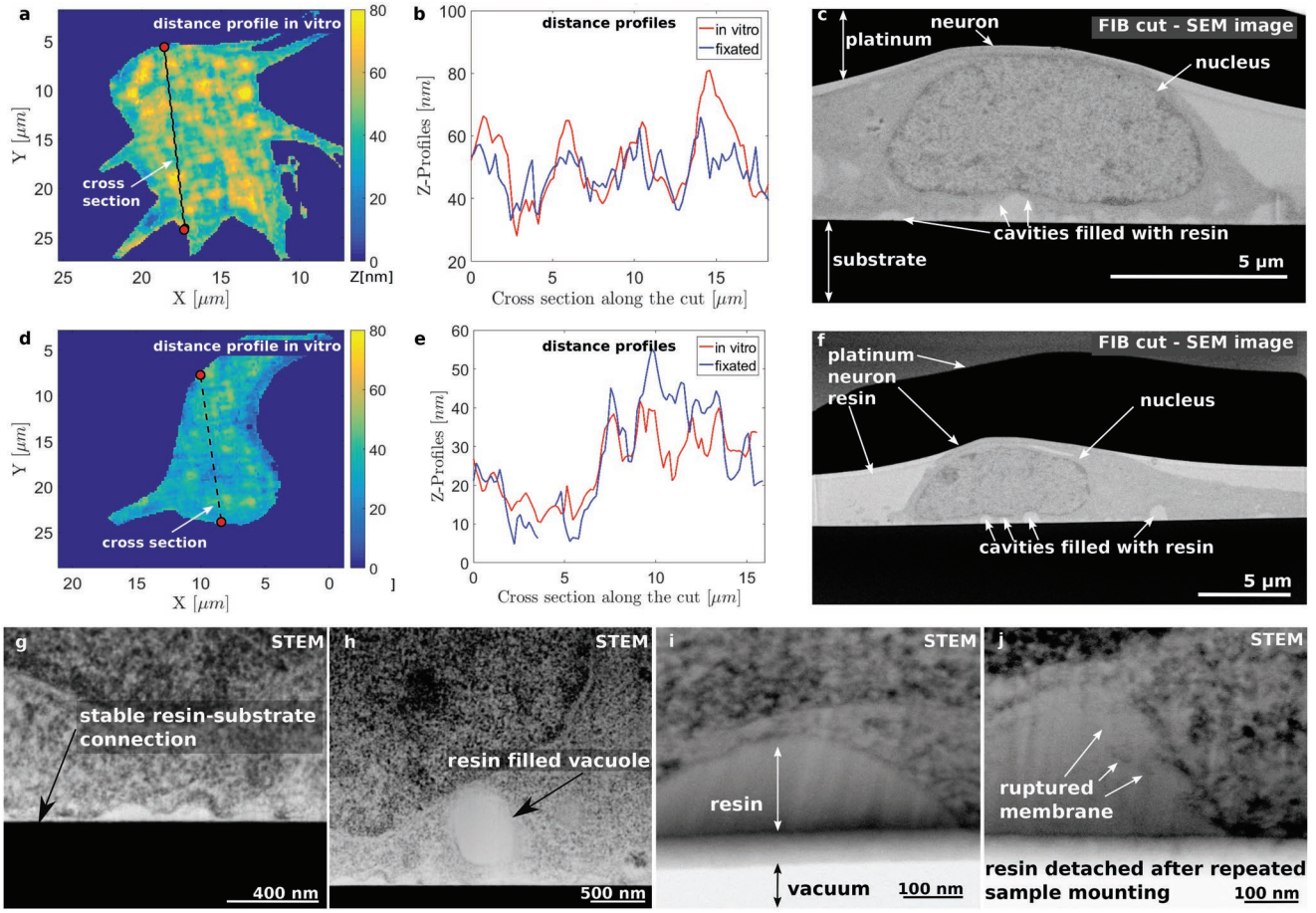

Figure 4. Correlation of SPRM and EM for two individual cells. The cell substrate distances are evaluated along the cross-section with SPRM and FIB-SEM and STEM for the same cells and in the same direction. a,d) The cell–substrate distance is plotted as area scans representing the situation in vitro. The cross-section is marked for the line-plot evaluations shown in (b)and (e). b,e) The distance is evaluated along the cross-section marked in (a) and (d), respectively, for the system before and after the fixation. c,f) An SEM-image taken after FIB sectioning along the cross-section marked in (a) and (d) reveals resin filled cavities at the cell–substrate interface. g) After extracting a lamella via FIB sectioning from the center of the cell shown in (d), the lamella was imaged with an STEM allowing for the resolution of the cell membrane. The close contacts found here are in good agreement with the SPRM results shown in (d) and (e). h) The high resolution of STEM allows us to discriminate between cavities at the interface and resin filled vacuoles as we see here. i) The STEM shows a cavity at the interface with an intact cell membrane. The resin was in contact with the substrate during the first mounting of the lamella (compare (f)). After the second mounting of the fragile lamella, the resin locally detached from the substrate. i,j) Therefore, the area underneath the resin appears white (vacuum) in the STEM. j) This cavity shows a ruptured cell membrane. The cell membrane might have been torn during the preparation process.

changes in cytosolic RI lead to a shift of the entire reflection curve, the plasmon resonance angle shifts toward higher angles in areas of cell adhesion, while in uncovered areas the plasmon resonance angle remains constant. Other reasons for the observation of local changes in the cell–substrate distance might be cell dynamics occurring during the time between the first measurement and the fixation (on average 2 h) as well as the changes introduced by the second mounting of the sample. Since our cell measurements are based on a scanning method, which usually includes more than 10 000 single-point measurements arranged on a grid with approximately 250 nm spacing between neighboring scanning points, repeating a cell measurement always results a collection of slightly shifted measurement points and thus never in the exact same results. As in this study the samples had to be taken out of the sample holder prior to fixation and reinstalled in the sample holder after the fixation, the changes in the scanning points is even more probable.

The lateral resolution in SPRM is defined by the spot size of the illuminated area during scanning, which is diffraction limited ($d \approx 200$ nm).[49,58,59] The values measured with SPRM thus correspond to the average cell–substrate distance within the illuminated areas. In wide cavities it is therefore to be expected that EM images may show larger maximum values compared to SPRM measurements, while cavities narrower than its lateral resolution cannot be resolved. This explains why some of the cavities appear in the EM images and not in the SPRM results. However, in STEM, we found a cavity wider than the lateral resolution of SPRM that does not appear in the corresponding measurements (see Figure 4j). The extensive preparation protocol carried out after fixation comprises 12 changes of the extracellular fluids (7x with EtOH, 5× with resin, both in increasing concentration) which result in diffusion processes across the cell membrane and therefore consecutive replacements of the intracellular fluids. This large number of diffusion

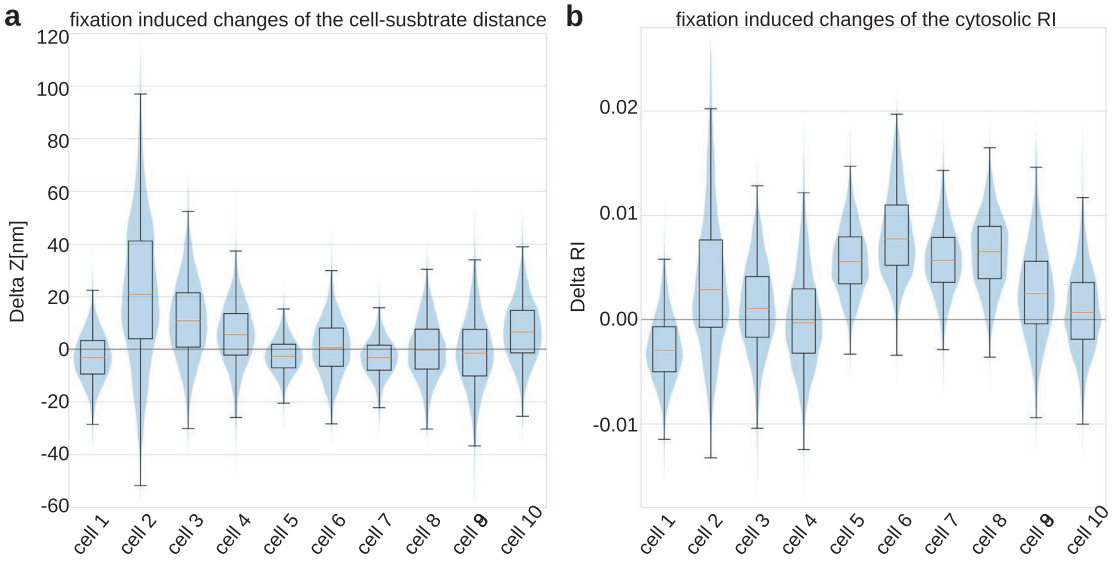

Figure 5. Fixation-induced changes in distance and refractive index. The changes in the cell–substrate distance and the cytosolic RI are evaluated for scanning point for 10 cells. a) We find prominent changes in the cell–substrate distance of cell 2 and cell 3 toward higher values while the remaining cells show random shifts. b) The cytosolic RI shows a systematic shift toward higher values after the fixation.

processes is likely to change the morphology of the cell membrane and thus the shape and size of the cavities. In particular, Figure 4j shows a partially ruptured membrane which indicates that the diffusion across the cell membrane may not have worked ideally and therefore, this cavity can be considered an artifact.

Both methods have their obvious advantages and disadvantages: FIB-STEM offers unique resolution in *x*- and *z*-direction and also resolves cell organelles, whereas SPRM can display the situation in the living cell. One limitation of SPRM is its specificity for sample structure and optical properties of materials within the sample. The exchange of water with resin both in the cell–substrate cleft and within the cell leads to a strong increase in the RI of the samples, making it impossible to investigate morphological changes caused by this preparation step. Furthermore, after exposing the cells to OsO_4 and uranyl acetate, the samples can only be handled in designated work areas and therefore not be further investigated with SPRM. However, the combination of these two methods allows us to benefit from all the above advantages in the same study.

4. Conclusion

We have shown a correlative workflow that enables us to complement FIB-S(T)EM studies with SPRM as an independent technique. This method has been successfully applied to a preparation protocol for cortical neurons. The comparison of the pre and post chemical fixation profiles of the adherent cell membrane allowed us to study the effects of chemical fixation on the cell–substrate distance. Our results showed a shift in the average cell–substrate distance of less than 10 nm for the vast majority of investigated cells without preferential directionality. This suggests that the chemical fixation required for electron microscopy could maintain the structure at the cell–substrate interface which dispels one of the main objections to electron microscopy. This comparison also allowed us to exclude those cells that show a significant shift in the cell–substrate distance from subsequent EM investigations. This increased the probability of the cells examined in FIB-STEM being preserved in their natural shape. Correlating SPRM data with electron microscopy images allowed us to identify artifacts most likely caused by sample preparation subsequent to fixation and highlight the regions with low probability of preparation artifacts. The discovered artifacts include torn membrane segments and cavities at the cell–substrate interface.

By excluding artifact affected regions, the described correlative workflow will allow future studies to focus in detail on regions that are in good agreement with the SPRM data in living cells. This increases the likelihood of mapping cell–substrate interaction which corresponds to the situation in the living cell enormously. The workflow can also serve to test and verify various fixation and preparation protocols in the future.

5. Experimental Section

SPRM: In the live-imaging mode, the sample was illuminated through the objective under the surface plasmon resonance angle using a projector as a light source. As a result, areas with close cell–substrate distance appeared brighter than areas with higher cell–substrate distances or the surrounding media (see Figures 1b and **6**a).

In scanning SPRM, we focus radially polarized laser light at the glass–gold interface which results in an illumination of the sample with p-polarized light under a broad range of angles. Most of the incident light is reflected at the interface and is captured by the objective whereas other parts of the incident light were absorbed and excite surface plasmons. An evanescent field is created which interacts with the material within the penetration depth. Based on a study by Peterson et al., we assume a penetration depth of $\approx d_p = 200$ nm for a wavelength of $\lambda = 633$ nm.[50] This means that the evanescent field interacts with the

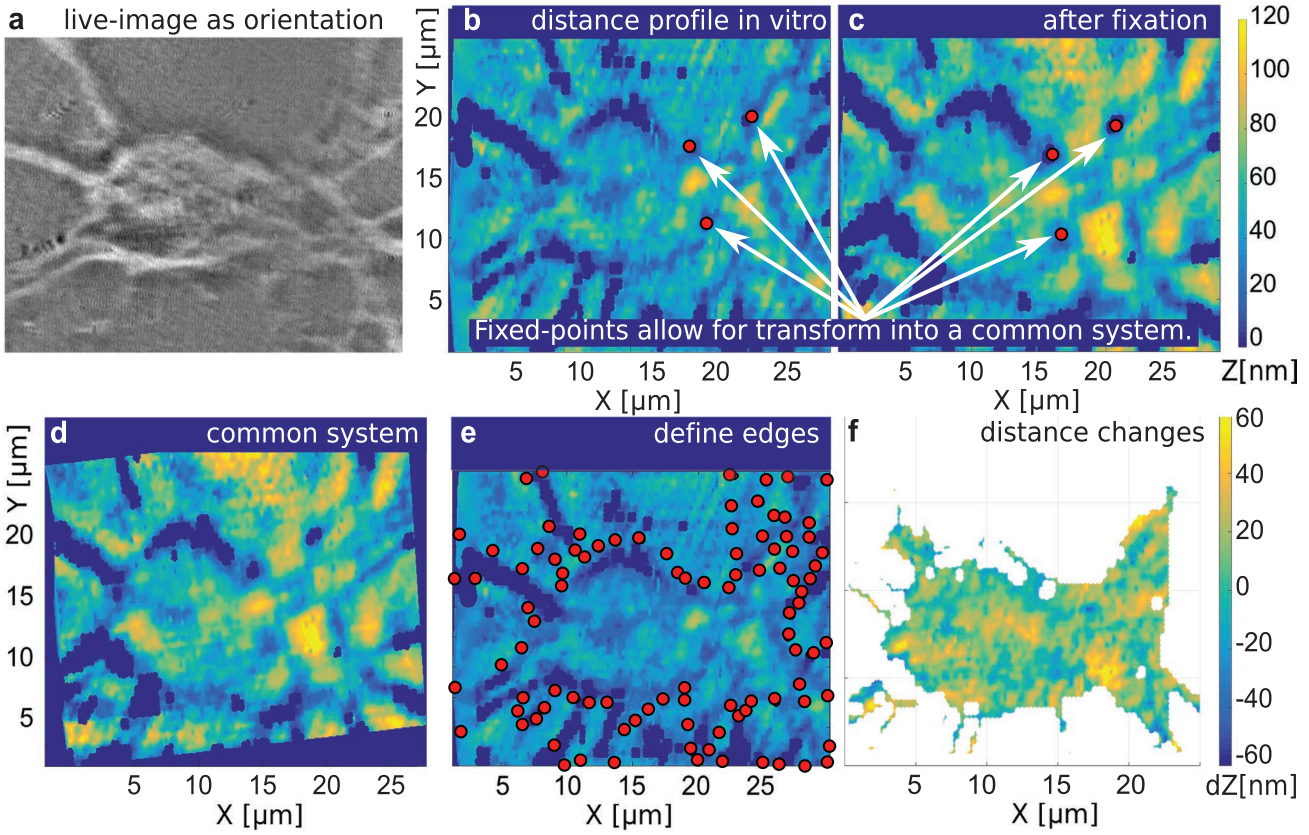

Figure 6. Working principle of the software align and compare. The software allows us to determine the fixation induced changes in the cell–substrate distance. a) An SPRM live-image of the cell allows us to identify the cell-adhesion areas. b,c) First, distance profiles before and after the fixation are shown in parallel and the user is asked to identify at least three salient points. d) Based on the coordinates of these points, a common coordinate system is determined. e) The edges of the cell adhesion area are defined by the user based on a bright field image in (a). f) The difference in the cell substrate distance before and after the fixation is determined and plotted as an area plot.

cell membrane at the interface and a small fraction of the cytoplasm but we cannot get insights into the properties of cellular material outside of this range. By capturing images of the BFP of the objective (see Figure 1e), the angle spectrum of the reflected light could be extracted (see Figure 1f). This data can be analyzed based on the transfer-matrix method. Here, the sample was modeled as a multilayer system with specific optical properties (see Figure 1d). The metal layers as well as the cell membrane were assumed constant whereas the thickness of the culture media layer as well as the intracellular RI were variable. These two variables were obtained by fitting the simulated curve to the data (see Figure 1f).[56] As a result of this analysis, a cell–substrate distance profile as well as the profile of the cytosolic RI were generated for each scan.

Align and Compare Software: The software align and compare was written in MATLAB and allowed us to determine the fixation induced changes in the cell–substrate distance and in the cytosolic RI. Before starting the align and compare-routine, the scanning data was analyzed as briefly described before.

This analysis was based on the description of the sample as a multilayer system. The reflectance of such a system can be described as a function of the angle of incidence using the transfer-matrix method.[64] As was shown before, this method can be used to analyze the intracellular RI separately from the cell–substrate distance by optimizing the overlay of the simulated and the measured reflectance.[56] As a result of this analysis, the cell–substrate distance as well as the RI were saved as individual data sets.

After this initial analysis, the cell–substrate distance profiles and RI profiles which correspond to the measurements before and after the fixation of the same cell were loaded into the align and compare routine. The software displays the distance profiles corresponding to the two states (see Figure 6b,c). Three salient points were now identified in the two distance profiles via graphical input. The coordinates of these inputs built the basis for the coordinate transform which enabled us to transform the scanning data of the two measurements into a common system. The coordinate transformation consisted of a shift and a rotation in the x–y plane. By applying this transformation, the data corresponding to the measurement were transferred after the fixation into the coordinate system of the first measurement (see Figure 6d). Afterward, the user was asked to mark the cell-adherence area in the scan based on graphical input. An SPRM live-image (see Figure 6a) helped to identify the respective areas. Now, a polygon including all the points entered by the user (see Figure 6e) was determined and the areas outside the polygon were discarded. Finally, the changes in the distance and RI inside the polygon were calculated point wise. These results were plotted in form of area plots (see Figure 6f), but also as line plots between two points chosen by the user via graphical input (see Figures 3 and 4a,b,d,e) as well as in the form of violin plots (see Figure 5) using Python.

Fixation and Preparation for FIB: The fixation, heavy metal stainings, and resin embeddings were carried out based on the protocol established by Belu et al.[7] Unless stated otherwise, all the chemicals were purchased from Sigma-Aldrich.

Chemical Fixation: First, the samples were rinsed three times with 37 °C warm PBS. The cells were fixed using 37 °C warm 3.2% glutaraldehyde solution at room temperature (RT) for 15 min. Afterward, the samples were washed three times with PBS at RT.

Staining with Osmium Tetroxide and Uranyl Acetate: The samples were rinsed twice with MilliQ at RT. Afterward, the samples were incubated with 1% OsO_4 in cacodylate buffer (Morphisto) for 2 h on ice. The samples were rinsed 5× with MilliQ before they were exposed to 1% tannic acid (Electron Microscopy Science) for 30 min at RT and again rinsed five times with MilliQ. Afterward, the samples were incubated with 2% uranyl acetate at 4 °C overnight and rinsed again five times with MilliQ.

Ethanol Dehydration: The cells were rinsed with gradual increasing ethanol (EtOH) series at RT: 5 min each with 10% EtOH, 30% EtOH, and 50% EtOH. 15 min with 70% EtOH, three times 5 min each with 90% EtOH and 95% EtOH, and finally 5 min with 100% EtOH.

Resin Embedding: The resin used for this embedding was prepared as follows: 20 mL DDSA was mixed with 12.5 mL of EPON 812 and 17.3 mL MNA was mixed with 15.2 mL EPON 812. Afterward, the two solutions were mixed. 1.3 mL of DMP30 was added to 32.5 mL of this mixture and stirred for 1 h.

The samples were exposed to resin–EtOH solutions with gradual increasing resin fraction at RT: The resin embedding was started by incubating the sample to a resin solution with 3:1 ratio (EtOH:resin) for 3 h, followed by 3 h incubation with a 2:1 solution, an overnight incubation with a 1:1 solution, a 3 h incubation with a 1:2 solution, a 3 h incubation with a 1:3 solution, and a 3 h incubation with pure resin. Afterward, EtOH was splashed repeatedly over the sample from the sides of the dish to remove the supernatant. Finally, the resin was cured at 60 °C for 12 h.

Metal Deposition: Before mounting the samples in the FIB-SEM system, a platinum layer was sputtered on the sample surface to avoid charging effects (using Balzer SCD004, 30 s, 30 mA).

Using a FIB-SEM system (Helios NanoLab 600i, FEI Co., Hillsboro, OR, USA), the cells were localized and an additional thin platinum layer was deposited on the region of interest via electron beam induced deposition to protect the sample from damages caused by the ion source. Before starting the FIB sectioning, an additional platinum layer of several micrometer thickness was deposited, which stabilized the sample during the FIB sectioning using ion beam induced deposition.

EM: The SEM imaging as well as the FIB sectioning were conducted on a Helios NanoLab 600i (FEI Co., Hillsboro, OR, USA). For STEM, a thin lamella (thickness at the cell–substrate interface ≈100 nm) was cut from the center of the cell and soldered to a TEM grid. The STEM imaging of the lamella was conducted on a Magellan 400 FESEM (FEI Co., Hillsboro, OR, USA) with electron beam energy of 28 keV and current of 0.1 nA. For high-contrast, high-resolution micrographs of an STEM II detector in bright field (BF) mode were used.

SPRM Sample Preparation: The samples consisted of a high index coverslip that was coated with a 3 nm thick chromium layer and a 38–40 nm thick gold layer. Specific markers that allowed for a unique identification of each position on the substrate were fabricated on top of the gold layer using photoresist. These substrates were glued to 35 mm polystyrene Petri dishes with a hole in the bottom and could afterward be used as substrates for cell culture.

Substrate Cleaning: Used substrates: High index coverslips (Olympus, HIGH INDEX-CG); Clean substrates with ethanol, aceton, and isopropanol (5 min each); O2-plasma cleaning; machine: Barrel Reactor TePla Gigabatch 310M; parameters: 200 W, 50 sccm, 5 min.

Chromium Deposition: 3 nm Cr sputtered; machine: Leybold Univex 450C; parameter: 300 W DC, 60 sccm Argon (2.1×10^{-2} mBar), 5.3 s.

Gold Deposition: Gold evaporation directly after the chromium deposition; machine: PLS-570; parameters: 38 nm Au.

Lithography: Baking of samples 5 min, 130 °C; Spincoating: AZ5214E: 4000 rpm; Baking of samples 1 min, 110 °C; Mask Aligner MA4: 2.3 s, 75 mW cm^{-2}, hard contact; machine: Süss MA/BA 8; Development: MIF326, 45 s, stop in DI-water ≈5 min until guide value >10 MOhm cm; Baking of samples 10 min, 135 °C.

Neuronal Cell Culture: 200 000 primary neurons were suspended in 2.5 mL and seeded on the PLL coated substrates. The entire media was replaced 3 h after plating.

Half the volume of the media was replaced each 3 or 4 days (alternating).

Culture Media: 10 mL Neurobasal Medium (from Life Technologies, 21103049); 100 µL B-27 supplement (from Life Technologies, 17504044); 25 µL L-glutamine (from Life Technologies, 25030024); 10 µL Gentamicin (from Sigma, G1397).

Declaration: The neurons were isolated from Wistar rat embryos on day 18 at the ICS-8 (approved by Landesumweltamt für Natur, Umwelt und Verbraucherschutz Nordrhein-Westfalen, Recklinghausen, Germany, number 84-02.04.2015.A173).

Acknowledgements

The authors thank Klaus Kreysing, Dr. Kristian Franze, and Dr. Moritz Kreysing for fruitful scientific discussions, Michael Prömpers for the sample production, and Bettina Breuer and Timm Hondrich for the neuron isolation.

Conflict of Interest

The authors declare no conflict of interest.

Author Contributions

E.K. conceived, executed, and evaluated the SPRM experiments, wrote the software align and compare, and wrote the manuscript. S.S. conceived and executed the heavy metal stainings and the resin embedding. H.H. wrote the SPRM analysis software. E.B.-R. and E.N. conceived and executed the FIB-S(T)EM experiments. A.O. supervised the project. All authors reviewed the manuscript.

Keywords

cell–substrate distance, electron microscopy, fixation artifacts, surface plasmon resonance microscopy

Received: November 25, 2019
Revised: December 13, 2019
Published online: January 28, 2020

[1] W. Chen, Y. Shao, X. Li, G. Zhao, J. Fu, *Nano Today* **2014**, *9*, 759.
[2] M. Ventre, P. A. Netti, *ACS Appl. Mater. Interfaces* **2016**, *8*, 14896.
[3] D. Iandolo, F. A. Pennacchio, V. Mollo, D. Rossi, D. Dannhauser, B. Cui, R. M. Owens, F. Santoro, *Adv. Biosyst.* **2018**, *3*, 1800103.
[4] S. P. Lacour, G. Courtine, J. Guck, *Nat. Rev. Mater.* **2016**, *1*, 16063.
[5] J. W. Salatino, K. A. Ludwig, T. D. Y. Kozai, E. K. Purcell, *Nat. Biomed. Eng.* **2017**, *1*, 862.
[6] W. Zhao, L. Hanson, H.-Y. Lou, M. Akamatsu, P. D. Chowdary, F. Santoro, J. R. Marks, A. Grassart, D. G. Drubin, Y. Cui, B. Cui, *Nat. Nanotechnol.* **2017**, *12*, 750.
[7] A. Belu, M. Yilmaz, E. Neumann, A. Offenhäusser, G. Demirel, D. Mayer, *J. Biomed. Mater. Res., Part A* **2018**, *106*, 1634.
[8] M. E. Spira, A. Hai, *Nat. Nanotechnol.* **2013**, *8*, 83.
[9] M. R. Angle, B. Cui, N. A. Melosh, *Curr. Opin. Neurobiol.* **2015**, *32*, 132.
[10] M. M. Stevens, J. H. George, *Science* **2005**, *310*, 1135.
[11] G. Wrobel, M. Holler, S. Ingebrandt, S. Dieluweit, F. Sommerhage, H. P. Bochem, A. Offenhausser, *J. R. Soc., Interface* **2008**, *5*, 213.

[12] A. Fendyur, N. Mazurski, J. Shappir, M. E. Spira, *Front. Neuroeng.* **2011**, *4*, 14.
[13] L. Hanson, Z. C. Lin, C. Xie, Y. Cui, B. Cui, *Nano Lett.* **2012**, *12*, 5815.
[14] Z. C. Lin, C. Xie, Y. Osakada, Y. Cui, B. Cui, *Nat. Commun.* **2014**, *5*, 3206.
[15] C. Py, D. Salim, R. Monette, T. Comas, J. Fraser, D. Martinez, M. Martina, G. Mealing, *Biotechnol. Bioeng.* **2011**, *108*, 1936.
[16] M. Wesche, M. Hüske, A. Yakushenko, D. Brüggemann, D. Mayer, A. Offenhäusser, B. Wolfrum, *Nanotechnology* **2012**, *23*, 495303.
[17] R. Wierzbicki, C. Købler, M. R. B. Jensen, J. Łopacińska, M. S. Schmidt, M. Skolimowski, F. Abeille, K. Qvortrup, K. Mølhave, *PLoS One* **2013**, *8*, e53307.
[18] F. Santoro, J. Schnitker, G. Panaitov, A. Offenhäusser, *Nano Lett.* **2013**, *13*, 5379.
[19] F. Santoro, S. Dasgupta, J. Schnitker, T. Auth, E. Neumann, G. Panaitov, G. Gompper, A. Offenhäusser, *ACS Nano* **2014**, *8*, 6713.
[20] A. Czeschik, P. Rinklin, U. Derra, S. Ullmann, P. Holik, S. Steltenkamp, A. Offenhäusser, B. Wolfrum, *Nanoscale* **2015**, *7*, 9275.
[21] A. Belu, J. Schnitker, S. Bertazzo, E. Neumann, D. Mayer, A. Offenhäusser, F. Santoro, *J. Microsc.* **2016**, *263*, 78.
[22] M. S. Lucas, M. Günthert, A. G. Bittermann, A. de Marco, R. Wepf, in *Correlative Light and Electron Microscopy III* (Eds: T. Müller-Reichert, P. Verkade), Methods in Cell Biology, Vol. 140, Academic Press, San Diego, CA **2017**, pp. 123–148.
[23] S. Seyock, V. Maybeck, E. Scorsone, L. Rousseau, C. Hébert, G. Lissorgues, P. Bergonzo, A. Offenhäusser, *RSC Adv.* **2017**, *7*, 153.
[24] F. Santoro, W. Zhao, L.-M. Joubert, L. Duan, J. Schnitker, Y. van de Burgt, H.-Y. Lou, B. Liu, A. Salleo, L. Cui, Y. Cui, B. Cui, *ACS Nano* **2017**, *11*, 8320.
[25] F. Santoro, Y. van de Burgt, S. T. Keene, B. Cui, A. Salleo, *ACS Appl. Mater. Interfaces* **2017**, *9*, 39116.
[26] H.-Y. Lou, W. Zhao, Y. Zeng, B. Cui, *Acc. Chem. Res.* **2018**, *51*, 1046.
[27] S. Seyock, V. Maybeck, A. Offenhäusser, *Micron* **2017**, *92*, 39.
[28] M. Dipalo, A. F. McGuire, H.-Y. Lou, V. Caprettini, G. Melle, G. Bruno, C. Lubrano, L. Matino, X. Li, F. De Angelis, B. Cui, F. Santoro, *Nano Lett.* **2018**, *18*, 6100.
[29] V. P. Collins, B. Arborgh, U. Brunk, *Acta Pathol. Microbiol. Scand., Sect. A* **1977**, *85A*, 157.
[30] M. J. Doughty, J. P. G. Bergmanson, Y. Blocker, *Tissue Cell* **1997**, *29*, 533.
[31] A. G. Bittermann, D. Schaer, M. Mitsi, V. Vogel, R. Wepf, *The 15th European Microscopy Congress*, Manchester Central, UK, September **2012**.
[32] F. Greve, S. Frerker, A. G. Bittermann, C. Burkhardt, A. Hierlemann, H. Hall, *Biomaterials* **2007**, *28*, 5246.
[33] T. F. Anderson, *Trans. N. Y. Acad. Sci.* **1951**, *13*, 130.
[34] A. Boyde, E. MacOnnachie, *Scanning* **1979**, *2*, 149.
[35] D. Schroeter, E. Spiess, N. Paweletz, R. Benke, *J. Electron Microsc. Tech.* **1984**, *1*, 219.
[36] D. Gusnard, R. H. Kirschner, *J. Microsc.* **1977**, *110*, 51.
[37] S. Seyock, A. Offenhäusser, M. Spehr, *Ph.D. Thesis*, RWTH Aachen University **2018**.
[38] T. E. Morgan, *J. Cell Biol.* **1967**, *32*, 757.
[39] D. Braun, P. Fromherz, *Phys. Rev. Lett.* **1998**, *81*, 5241.
[40] H. Sorribas, D. Braun, L. Leder, P. Sonderegger, L. Tiefenauer, *J. Neurosci. Methods* **2001**, *104*, 133.
[41] A. I. Chizhik, J. Rother, I. Gregor, A. Janshoff, J. Enderlein, *Nat. Photonics* **2014**, *8*, 124.
[42] R. Alford, H. M. Simpson, J. Duberman, G. C. Hill, M. Ogawa, C. Regino, H. Kobayashi, P. L. Choyke, *Mol. Imaging* **2009**, *8*, 7290.2009.00031.
[43] U. Kubitscheck, *Fluorescence Microscopy: From Principles to Biological Applications*, 2nd ed., Wiley-Blackwell, Weinheim **2017**.
[44] K.-F. Giebel, C. Bechinger, S. Herminghaus, M. Riedel, P. Leiderer, U. Weiland, M. Bastmeyer, *Biophys. J.* **1999**, *76*, 509.
[45] B. Huang, F. Yu, R. N. Zare, *Anal. Chem.* **2007**, *79*, 2979.
[46] S. A. Kim, K. M. Byun, J. Lee, J. H. Kim, D.-G. A. Kim, H. Baac, M. L. Shuler, S. J. Kim, *Opt. Lett.* **2008**, *33*, 914.
[47] W. Wang, Y. Yang, S. Wang, V. J. Nagaraj, Q. Liu, J. Wu, N. Tao, *Nat. Chem.* **2012**, *4*, 846.
[48] K. Watanabe, K. Matsuura, F. Kawata, K. Nagata, J. Ning, H. Kano, *Biomed. Opt. Express* **2012**, *3*, 354.
[49] K. Toma, H. Kano, A. Offenhäusser, *ACS Nano* **2014**, *8*, 12612.
[50] A. W. Peterson, M. Halter, A. Tona, A. L. Plant, *BMC Cell Biol.* **2014**, *15*, 35.
[51] K. Syal, W. Wang, X. Shan, S. Wang, H.-Y. Chen, N. Tao, *Biosens. Bioelectron.* **2015**, *63*, 131.
[52] Y. Yang, H. Yu, X. Shan, W. Wang, X. Liu, S. Wang, N. Tao, *Small* **2015**, *11*, 2878.
[53] C.-T. Yang, R. Méjard, H. J. Griesser, P. O. Bagnaninchi, B. Thierry, *Anal. Chem.* **2015**, *87*, 1456.
[54] F. Zhang, S. Wang, L. Yin, Y. Yang, Y. Guan, W. Wang, H. Xu, N. Tao, *Anal. Chem.* **2015**, *87*, 9960.
[55] X.-W. Liu, Y. Yang, W. Wang, S. Wang, M. Gao, J. Wu, N. Tao, *Angew. Chem., Int. Ed.* **2017**, *56*, 8855.
[56] E. Kreysing, H. Hassani, N. Hampe, A. Offenhäusser, *ACS Nano* **2018**, *12*, 8934.
[57] A. W. Peterson, M. Halter, A. Tona, A. L. Plant, J. T. Elliott, *Plasmonics in Biology and Medicine XV*, Vol. *10509*, SPIE, San Francisco, CA, USA **2018**, https://doi.org/10.1117/12.2290776.
[58] K. Watanabe, N. Horiguchi, H. Kano, *Appl. Opt.* **2007**, *46*, 4985.
[59] H. Hassani, E. Kreysing, *Opt. Lett.* **2019**, *44*, 1359.
[60] J. Bozzola, *Electron Microscopy: Principles and Techniques for Biologists*, Jones and Bartlett, Sudbury, MA **1999**.
[61] B. Alberts, A. Johnson, D. Morgan, M. Raff, K. Roberts, P. Walter, *Molecular Biology of the Cell*, Garland Science, Taylor and Francis Group, New York, NY **2015**.
[62] G. M. Hale, M. R. Querry, *Appl. Opt.* **1973**, *12*, 555.
[63] T. L. McMeekin, M. L. Groves, N. J. Hipp, *Adv. Chem.* **1964**, *44*, 54.
[64] M. Born, E. Wolf, *Principles of Optics : Electromagnetic Theory of Propagation, Interference and Diffraction of Light*, Cambridge University Press, Cambridge, NY **1999**.